Gain-Scheduled H∞ for Vehicle High-Level Motion Control

Moad Kissai, Bruno Monsuez, Adriana Tapus, Xavier Mouton, Didier Martinez

Gain-Scheduled $\mathcal{H}_\infty$ for Vehicle High-Level Motion Control

Moad Kissai
ENSTA ParisTech
828 Boulevard des Maréchaux
91120 Palaiseau, France
moad.kissai@ensta-paristech.fr

Bruno Monsuez
ENSTA ParisTech
828 Boulevard des Maréchaux
91120 Palaiseau, France
bruno.monsuez@ensta-paristech.fr

Adriana Tapus
ENSTA ParisTech
828 Boulevard des Maréchaux
91120 Palaiseau, France
adriana.tapus@ensta-paristech.fr

Xavier Mouton
Group Renault
1 Avenue du Golf
78280 Guyancourt, France
xavier.mouton@renault.com

Didier Martinez
Group Renault
1 Avenue du Golf
78280 Guyancourt, France
didier.d.martinez@renault.com

ABSTRACT

Vehicle motion control has many challenges to overcome. One of the main problems is robustness against not only environmental changes but also uncertainties about the vehicle itself. This paper focuses on this problem using robust control design at the control architecture's high level. Researches tend to decentralize the control to treat longitudinal and lateral dynamics separately. Here, an overall vehicle model is first proposed and studied to justify the structure that the high-level controller should embrace. Co-simulation results of different combinations showed promising performances to face uncertainties and couplings. Therefore, robust techniques combined with control allocation techniques may enhance autonomous vehicles reliability.

CCS Concepts

•**Computer systems organization** → **Robotic control;** *Embedded systems;* •**Applied computing** → Engineering;

Keywords

$\mathcal{H}_\infty$ Control; Gain Scheduling; Control Allocation; Vehicle Dynamics; Robustness; Co-Simulation.

1. INTRODUCTION

The automotive sector is changing. Autonomous vehicles are gathering different stakeholders that were formerly far from mobility problems. For ground vehicles, performances are closely related to the tire/road interface. In fact, tires are the only effectors that make vehicles move [1]. However, neither tire forces nor the friction coefficient are measured in real time in commercial vehicles. Moreover, even vehicle parameters are uncertain, e.g. the overall mass [2] or the tires' cornering stiffness [3]. Motion control performances should stay acceptable whether there is only the driver in the car or with other passengers, and in different type of roads. All stakeholders should be sensitized to these physical challenges. Robust control becomes then an important requirement to be fulfilled by active chassis systems. Design of robust controllers depends on the augmented plant model. For example, in the conventional $\mathcal{H}_\infty$ design, the order of the controller resulting is equal to the number of states in the plant plus the number of states in the requirements weights plus twice the number of states in feedthrough matrix [4]. For high-order plants, the controller generated by such design procedures is not implementable. The common practice is to then consider a reduced plant model that depicts only the important dynamics. In this context, in [1], a Relative Gain Array (RGA) study has been conducted to evaluate the system couplings near the crossover frequency using a simplified four-wheeled vehicle equipped by an Electronic Stability Program (ESP) and an Electric Power Assisted Steering (EPAS). Authors concluded that the system can be decoupled for high frequencies. Youla parameterization has been used then for each Single-Input Single-Output (SISO) transfer function. Results were acceptable for each variable only when the throttle was on, which means with the presence of a driver to control the longitudinal speed. Authors in [5] proposed a Sliding Mode Control (SMC) to coordinate the ESP and active steering devices, both in front and rear. The bicycle model has been chosen to design the controller. Two objectives has been pursued: maneuverability by means of yaw rate tracking, and lateral stability by minimizing the side-slip angle. A four-wheeled vehicle model has been considered afterwards in the low-level control for the ESP. Couplings were not managed at the high-level control as two different vehicle model have been considered. Moreover, no lateral velocity control have been ensured whereas a vehicle equipped by Active Front and Rear Steering (AFS & ARS) can ensure a lateral transitional motion to avoid an

ICCMA 2018, October 12–14, 2018, Tokyo, Japan
ACM ISBN 978-1-4503-6563-5…$15.00
DOI: 10.1145/3284516.3284544

obstacle for example. SMC was used also in [6] to control an electric vehicle equiped by a 4-Wheel Steering (4WS) system and a 4-Wheel Drive (4WD) system. A four-wheeled vehicle model was considered, but only to control the lateral dynamics of the vehicle. Couplings with the longitudinal dynamics were then ignored. In [7], a Linear with Parameters Varying (LPV)/$\mathcal{H}_\infty$ controller has been chosen as the high-level controller for a vehicle equipped by AFS and rear braking. Although good robustness is ensured, again, only a bicycle model was considered to design the controller. A 14-Degrees Of Freedom (DOF) full vehicle model equipped by an AFS, an Anti-lock Braking System (ABS), and Semi-Active Suspension (SAS) has been used in [8] and then simplified for control synthesis. A high-level controller based on SMC has been chosen. As the authors noted, the SMC procedure suffers from high-frequency chattering. The sign function can be used instead of the saturation function [8] to reduce the effect of chattering. We believe that this method is more suited for electronic devices, and in contrast, could accelerate mechanical actuators aging or tire wear.

The state of art shows that either we employ complex robust controllers based on simplified non-coupled vehicle models, or we decouple a complex vehicle model to use simplified controllers at each direction. In this paper, we privilege neither the first nor the second approach. We rather investigate a new approach where we use a relatively complex robust high-level controller based on a relatively complex four-wheeled vehicle model with an optimal coordination strategy. The goal is to evaluate the dynamic couplings at the vehicle level to justify the structure of the high-level controller. A full vehicle model equipped by an ESP, an ARS, and Rear Torque Vectoring (RTV) is first developed. A linear tire model with varying parameters is also used. A pre-study is carried out to evaluate the dynamic couplings. Different robust high-level controllers are compared using the same control allocation strategy by means of co-simulation of Matlab/Simulink® and AMESim®. Results have shown different behaviors for low and high speed maneuvers. Therefore, a Gain-Scheduled $\mathcal{H}_\infty$ controller seems to be a better choice for the vehicle's high level control.

The rest of the paper is structured as follows: We start in Section 2 by presenting the vehicle model considered for the dynamic couplings study. In Section 3, the high-level controllers chosen for comparison are described. The common control allocation strategy used is briefly presented in Section 4. Section 5 presents results obtained by co-simulation of Matlab/Simulink® and AMESim®. A discussion about robustness challenges and the relevance of this work is provided in Section 6. Conclusions and future works are outlined in Section 7.

2. VEHICLE MODELING

In this work, we focus on the high-level controller for over-actuated vehicles. The vehicle model should depict the dynamic couplings that could hamper a coordinated motion. A full vehicle model is then considered in this Section. Using Newton's laws of motion, and simplifying cross-multiplied low angles and angular velocities, e.g. multiplication of the roll velocity and the pitch velocity, we find the following state-space representation:

$$\begin{cases} \dot{V}_x = \dfrac{F_{x_{tot}}}{M} + \dfrac{M_s}{M} g V_x + V_y \dot{\psi} & (1) \\ \dot{V}_y = \dfrac{F_{y_{tot}}}{M} - V_x \dot{\psi} & (2) \\ \dot{V}_z = \dfrac{F_{z_{tot}}}{M} & (3) \\ \ddot{\phi} = \dfrac{M_{x_{tot}}}{I_{s_{xx}}} - \dfrac{K_r}{I_{s_{xx}}}\phi - \dfrac{C_{s_r}}{I_{s_{xx}}}\dot{\phi} & (4) \\ \ddot{\theta} = -\dfrac{M_s h_s}{M I_{s_{yy}}} F_{x_{tot}} + \dfrac{M_{y_{tot}}}{I_{s_{yy}}} - \dfrac{M K_p + M_s^2 h_s g}{M I_{s_{yy}}}\theta & (5) \\ \quad - \dfrac{C_{s_p}}{I_{s_{yy}}}\dot{\theta} & (6) \\ \ddot{\psi} = -\dfrac{M_s h_s}{M I_{zz}} \phi F_{x_{tot}} + \dfrac{M_{z_{tot}}}{I_{zz}} & (7) \end{cases}$$

With V_x, V_y, V_z are the longitudinal, lateral and the vertical velocity of the vehicle respectively. ϕ, θ, ψ are the roll, pitch, and yaw angle of the vehicle. M_s and M are the vehicle's sprung and overall masses, h_s is the height of the vehicle's center of gravity, g is the gravitational acceleration, K_r is the equivalent overall antiroll bar stiffness, C_{s_r} is the equivalent overall roll suspension damping, and K_p and C_{s_p} are the equivalent overall pitch suspension stiffness and damping. $I_{s_{xx}}$ and $I_{s_{yy}}$ are the sprung mass's roll and pitch moment of inertia and I_{zz} is the vehicle's yaw moment of inertia. $F_{i_{tot}}$ and $M_{i_{tot}}$ are the combination of tire forces and moments projected at the axis "i".

This model has been validated using a high-fidelity vehicle model provided by LMS Imagine.Lab AMESim®. This latter has 15 DOF. Complex axle kinematics are used to model the specific joint between sprung and unsprung masses. Regarding the validation procedure, we make use of a driver model provided by LMS Imagine.Lab AMESim® and designed using Model Predictive Control (MPC) to track a path with adapted velocity profile. This is carried out on a 3D reproduction of the approved International Circuit of Magny-Cours. The trajectory tracked at high velocities is illustrated in Fig. 1. Simulations of this severe maneuver are shown in Fig. 2. As we can in Fig. 2, the model shows

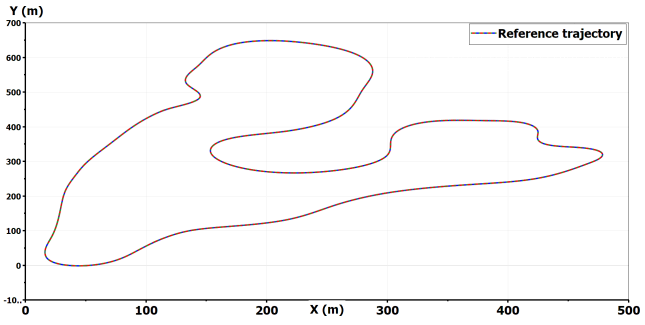

Figure 1: Magny-Cours trajectory.

good precision for all states in a coupled maneuver. The effect of slopes was also taken into account. This model can then be chosen as a starting model for all Global Chassis Control (GCC) synthesis. It is important to start with a complex full vehicle model and then reduce it while justifying each simplification. Starting with a simplified model, as

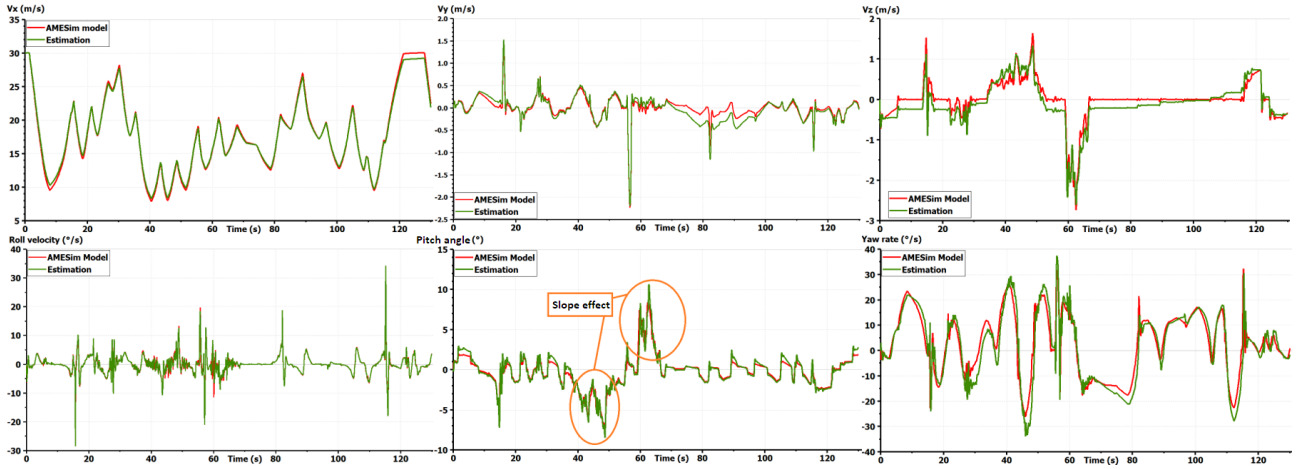

Figure 2: Validation of the vehicle model.

the bicycle model, could lead to the ignorance of important dynamics and couplings making the control fail.

In our case, the vehicle model is equipped by an Electronic Stability Program (ESP), an Active Rear Steering (ARS), and a Rear Torque Vectoring (RTV) system. The goal is also to study subsystems' interactions in over-actuated vehicles, especially when steering and traction are done in the same axle. As no active suspensions are considered, related vertical states are not necessary for control synthesis. However, the effect of the vertical load on tire stiffness should be taken into account. This is ensured by means of the linear tire with varying parameters described in subsection 3.3. The vehicle model becomes then:

$$\begin{cases} \dot{V}_x = \dfrac{F_{x_{tot}}}{M} + V_y\dot{\psi} & (8) \\ \dot{V}_y = \dfrac{F_{y_{tot}}}{M} - V_x\dot{\psi} & (9) \\ \ddot{\psi} = \dfrac{M_{z_{tot}}}{I_{zz}} & (10) \end{cases}$$

As it can be seen, the model is quasi-linear with varying parameters. Effects of the off-diagonal terms should be studied before determining the high-level controller nature.

3. HIGH-LEVEL CONTROL

To study the dynamic couplings using classical methods, we first linearize the vehicle model. This is usually done by employing a Taylor series expansion around a nominal system trajectory representing the operating points [1]. Using the Jacobean matrix, the model becomes then:

$$\begin{bmatrix} \dot{V}_x \\ \dot{V}_y \\ \ddot{\psi} \end{bmatrix} = \begin{bmatrix} 0 & \dot{\psi}_e & V_{y_e} \\ -\dot{\psi}_e & 0 & -V_{x_e} \\ 0 & 0 & 0 \end{bmatrix} \begin{bmatrix} V_x \\ V_y \\ \dot{\psi} \end{bmatrix} + \begin{bmatrix} \frac{1}{M} & 0 & 0 \\ 0 & \frac{1}{M} & 0 \\ 0 & 0 & \frac{1}{I_{zz}} \end{bmatrix} \begin{bmatrix} F_{x_{tot}} \\ F_{y_{tot}} \\ M_{z_{tot}} \end{bmatrix} \quad (11)$$

Where V_{x_e}, V_{y_e}, and $\dot{\psi}_e$ are the longitudinal velocity, lateral velocity, and yaw rate at the operating point respectively. Two pre-studies are carried out before presenting robust control design: the Relative Gain Array (RGA), and Bode diagrams.

3.1 The Relative Gain Array (RGA)

Here, we aim to quantify interactions between inputs and outputs of a Multi-Inputs Multi-Outputs (MIMO) system. The most commonly used technique is the *Relative Gain Array (RGA)* developed by Bristol [9]. It helps the controller designer to decide a suitable input/output pairing for the MIMO system, and also gives few hints on pairings to avoid. Let $\mathbf{G}$ be a non-singular square complex general transfer matrix. The RGA of $\mathbf{G}$ is defined as:

$$RGA(\mathbf{G}(\mathbf{i}\omega)) = \mathbf{\Lambda}(\mathbf{G}(\mathbf{i}\omega)) = \mathbf{G}(\mathbf{i}\omega) \circ \left(\mathbf{G}(\mathbf{i}\omega)^{-1}\right)^t \quad (12)$$

Where "$\circ$" denotes the Hadamard product[1], the superscript "^{t}" denotes the matrix transpose, and ω the considered frequency. Note that the RGA depends on this latter. Therefore, it should be calculated at the crossover frequency chosen by designer. Discussion about the frequency is provided after the Bode diagrams study. Rules are simple: prefer pairings so that Λ_{ij} is close to 1, and avoid pairings with negative Λ_{ij}. In our case, we use vehicle parameters of a Renault Talisman[2] to first generate a global transfer matrix, and then calculate its RGA. For a crossover frequency of 1Hz (or 2πrad/s), we obtain the following matrix:

$$\mathbf{\Lambda}(\mathbf{G}(\mathbf{i}2\pi)) = \begin{bmatrix} 1 & 0 & 0 \\ 0 & 1 & 0 \\ 0 & 0 & 1 \end{bmatrix} \quad (13)$$

Which means that the system can be decoupled for a crossover frequency of 1Hz as the study in [1] have shown, by favoring diagonal pairings. However, for low frequencies, for example 10^{-2}rad/s, we find:

$$\mathbf{\Lambda}(\mathbf{G}(\mathbf{i}2\pi)) = \begin{bmatrix} 0.05 & 0.95 & 0 \\ 0.95 & 0.05 & 0 \\ 0 & 0 & 1 \end{bmatrix} \quad (14)$$

Which means that off-diagonal terms should be prioritized for both longitudinal and lateral velocities. A study in the

[1]Known as elements-by-elements multiplication.
[2]Parameters provided by the Group Renault itself.

frequency domain should be then carried out.

3.2 Bode Diagrams

To study the importance of frequency for dynamic couplings, we plot bode diagrams corresponding to the linearized model (11). Fig 3,4,5 show Bode diagrams for the longitudinal velocity, the lateral velocity, and the yaw rate respectively. Bode diagrams confirm the RGA study. In fact, for

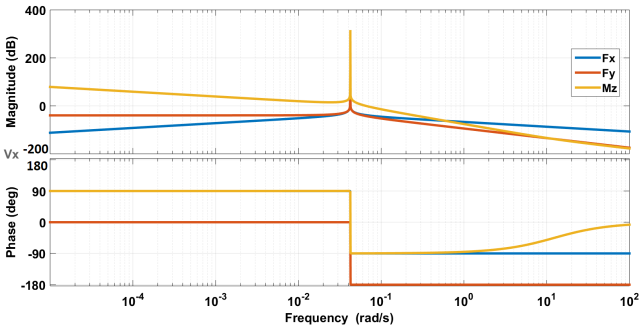

Figure 3: Bode diagrams for the longitudinal velocity.

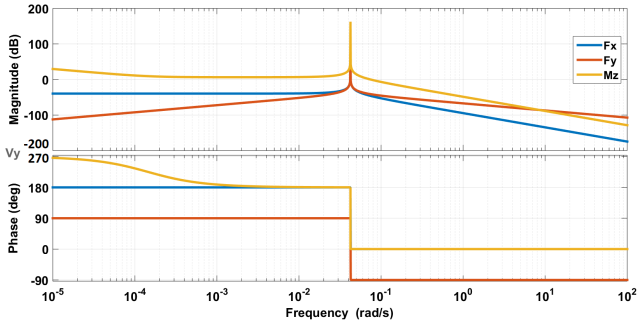

Figure 4: Bode diagrams for the lateral velocity.

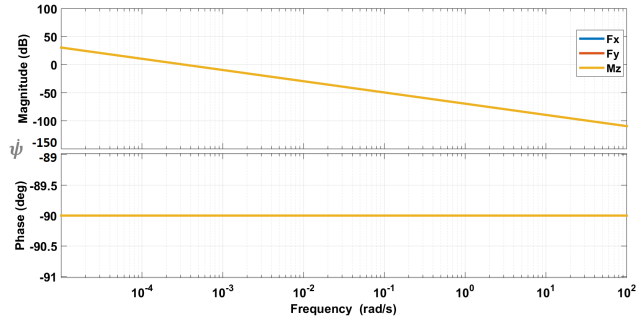

Figure 5: Bode diagrams for the yaw rate.

frequencies higher than 10rad/s, the influence of $F_{x_{tot}}$ on V_x and $F_{y_{tot}}$ on V_y are preponderant with respect to other inputs. The inverse is observed for low frequencies. The yaw rate can be decoupled for both low and high frequencies.

This imposes additional requirement for the high-level controller. In addition of performance and stability, a decoupled controller is preferred for easy tuning. In that case, the crossover frequency should be higher than 10rad/s.

3.3 Controller Design

As we discussed in the introduction, several robust techniques exist, e.g. the Sliding Mode Controller that got recently a lot of attention [5],[6],[8],[10]. This technique however still suffers from several problems as chattering [8]. An optimal design would be preferable. In this context, $\mathcal{H}_\infty$ based design presents several advantages. This technique allows the designer to express explicitly system uncertainties. $\mathcal{H}_\infty$ drawbacks could be overcome, in one hand, by a different design procedure as it would be shown, and in the other hand, by adding a gain scheduling characteristic.

3.3.1 Fixed-structure $\mathcal{H}_\infty$ synthesis

The main drawback in an $\mathcal{H}_\infty$ control design is the high order of the resulting controller. The order of the controller resulting is equal to the number of states in the plant plus the number of states in the requirements weights plus twice the number of states in the feedthrough matrix [4]. Here a different methodology is adopted.

In the conventional method [11], we first express an augmented plan taking into account tracking errors, control inputs, reference signals, external forces and noises. MIMO performance objectives are then formulated, and weighting functions are defined according to these objectives and added to the augmented system in order to enforce the controller to respect all the objectives. Dynamic or parametric uncertainties can also be added to the augmented plant in order to generate a valid controller to a set of systems and not only the nominal system. This of course enhance the controller robustness, but could however lead to the conservatism of the controller performances. A too big augmented plant could lead to a too high-order controller, and too many objectives to fulfill could lead to performance conservatism.

Therefore here, first we by-pass the augmented plant step and we keep only the system (11), and second, we do not express explicitly the uncertainties. Parameters like tire stiffness are highly nonlinear, and it is hard to define a range of variation of such parameters without penalizing the controller performance. This will rather be managed by gain scheduling for vehicle parameters, and adaptive control allocation for tire parameters using a new linear with varying parameters tire model [12]. This model takes into account the combined slip phenomenon because the tires can be solicited both longitudinally and laterally. It is precise enough in stable operating points, but also simple enough to be used in real-time control maneuvers. Details and validation through AMESim© is provided in [12]. We recall here the main results. Tire forces are expressed using varying stiffnesses, taking into account couplings, vertical forces influence, and friction influence.

$$\begin{cases} F_x = C_s^*(\alpha, \mu, F_z)\,\kappa & (15) \\ F_y = C_\alpha^*(\kappa, \mu, F_z)\,\alpha & (16) \end{cases}$$

where κ is the longitudinal slip, α is the side-slip, μ is the friction coefficient and F_z is the vertical load. $C_s^*(\alpha, \mu, F_z)$ and $C_\alpha^*(\kappa, \mu, F_z)$ are the tire varying longitudinal and cornering stiffness with respect to the corresponding varying parameters. Detailed expressions of the varying stiffness can be also found in [13]. In order to respect the friction ellipse concept described in [14], which describes penalization be-

tween tire forces, dynamic constraints are added [12]:

$$\begin{cases} F_x \leq \sqrt{(\mu F_z)^2 - F_y^2} & (17) \\ F_y \leq \sqrt{(\mu F_z)^2 - F_x^2} & (18) \end{cases}$$

Nevertheless, we add a new requirement to the control design problem, which is the fixed-structure of the controller. An additional effort from the control designer is required. The plant should be studied before choosing between coupled or decoupled control, PID or PI or phase-lag structure, and so on. This is the goal of the pre-study presented before. According to Fig. 3,4,5, a diagonal controller can be chosen as long as the imposed crossover frequency is higher than 10rad/s. Moreover, we choose the PI structure for each variable due their integral characteristic at higher frequencies. Six tunable parameters are then chosen in the control design problem. The optimal design algorithm is operated using Matlab®. Both methods can be tested. The conventional method is ensured by the Matlab function "*hinfsyn*" and the fixed-structure method by the function "*hinfstruct*". In this latter, to mitigate the risk of local minima, one could run several optimizations started from randomized initial values of tunable parameters. For more details, see [15].

Regarding performance weighting functions, closed loop shaping is used for defining control design requirements as in [7]. Two objectives are selected: tracking performance, and commands moderation. For tracking performance, we choose a steady-state offset less than 1%, a closed-loop bandwidth higher than 10Hz, and an amplification of high-frequency noise less than a factor 2, which give the weighting function:

$$W_{perf} = \frac{1}{2} \frac{\frac{s}{2\pi 10} + 2}{\frac{s}{2\pi 10} + 0.01} \quad (19)$$

With s is the Laplace operator. Regarding commands moderation, we use a static gaing representing the inverse of the maximum effort, which gives:

$$W_{act} = \frac{1}{1.2Mg} \quad (20)$$

Here we suppose that the maximum friction coefficient is equal to 1.2. The optimization algorithm gives the minimum $\mathcal{H}_\infty$ norm $\gamma = 1.14$ which proves that the different constraints are respected and the high-level controller is stable.

3.3.2 Gain-scheduled $\mathcal{H}_\infty$

One weakness in the preceding design is the dependency on the operating points used to linearize the plant model. For different operating points, different controller parameters values are generated, which influence the controller performance. A proper way to proceed would be to consider different stable operating points and make the controller parameters change with respect to these operating points. This is called scheduling. This consists on considering the nonlinearities in a system as varying parameters. Different linear controllers are designed for each value of the varying parameters. The controller parameters are after automatically adjusted as a function of the varying parameters. In our case, the model (11) is again used. The difference is that V_{x_e}, V_{y_e}, and $\dot{\psi}_e$ are now considered as varying parameters. As these parameters are also state variables, the system is now quasi-linear with varying parameters, which is more challenging [16].

The same performances cited in the previous paragraph are pursued for each set of scheduling parameters. The same $\mathcal{H}_\infty$ solver also is used for controller robustness. Three-dimensional lookup tables are then generated for each controller parameter. A gain-scheduled $\mathcal{H}_\infty$ controller is then used as [7]. The main difference in the control procedure in the chosen scheduling variables. In [7] a stability index is used to coordinate the subsystems. Here, scheduling is used for dynamic couplings management. Coordination is ensured by optimization-based control allocation techniques.

4. CONTROL ALLOCATION

Autonomous vehicles are expected to replace the human driver. For this purpose, more and more chassis systems are integrated in a single vehicle to improve the vehicle's safety so it can operate by itself. Coordination is becoming more challenging as unpredictable conflicts may arise. In [13], it has been shown that the coordination problem should be separated from the control problem. The architectures' review showed that a multi-hierarchical architecture is preferred where the mentioned problems are separated. As the vehicle is becoming over-actuated, optimization-based control allocation strategies should be adopted to coordinate chassis systems. The control allocation method is briefly presented here. The problem can be defined as follows [17]: find the control vector, $\vec{u} \in \mathbb{R}^n$ such that

$$\mathbf{B}\vec{u} = \vec{v} \quad (21)$$

subject to

$$\vec{u}_{min} \leq \vec{u} \leq \vec{u}_{max} \quad (22)$$

where $\mathbf{B} \in \mathbb{R}^{m \times n}$ is a control effectiveness matrix, $\vec{v} \in \mathbb{R}^m$ are the desired accelerations, n is the number of control effectors, and m is the number of axes to control with $n > m$. In our case, the vehicle is equipped by an ESP, ARS, and RTV. The problem can be defined as follows:

$$\begin{bmatrix} F_{x_{tot}} \\ F_{y_{tot}} \\ M_{z_{tot}} \end{bmatrix} = \begin{bmatrix} \cos(\delta_f) & \cos(\delta_f) & \cos(\delta_r) & \cos(\delta_r) & -\sin(\delta_r) \\ \sin(\delta_f) & \sin(\delta_f) & \sin(\delta_r) & \sin(\delta_r) & \cos(\delta_r) \\ b_{3,1} & b_{3,2} & b_{3,3} & b_{3,4} & b_{3,5} \end{bmatrix} \begin{bmatrix} F_{x_{fl}} \\ F_{x_{fr}} \\ F_{x_{rl}} \\ F_{x_{rr}} \\ F_{y_r} \end{bmatrix} \quad (23)$$

Where $b_{3,1} = l_f \sin(\delta_f) - \frac{t_f}{2}\cos(\delta_f)$, $b_{3,2} = l_f \sin(\delta_f) + \frac{t_f}{2}\cos(\delta_f)$, $b_{3,3} = -l_r \sin(\delta_r) - \frac{t_r}{2}\cos(\delta_r)$, $b_{3,4} = -l_r \sin(\delta_r) + \frac{t_r}{2}\cos(\delta_r)$ and $b_{3,5} = -l_r \cos(\delta_r)$

And $F_{x_{i,j}}$ is the $i-j$ braking force, where "i" is front or rear, and "j" is right or left, δ_i is the steering angle, l_i is the distance between the axle "i" and the vehicle's CoG, and t_i is the vehicle's track.

Regarding the online solver, the Weighted Least Squares (WLS) based on one stage Active Set Algorithm is used [18]. The reader can refer to [17],[18],[19] for further details on solver algorithms and their comparison.

5. CO-SIMULATION RESULTS

We choose the ISO 3888-1:1999(E) Double Lane-Change to test the different controllers. To give reliable results, control algorithms have been written in Matlab®, while a high-fidelity vehicle model equipped by an ESP, ARS, and RTV systems has been developed in LMS Imagine.Lab AMESim®. Simulink is used as a bridge to co-simulate Matlab's high performance algorithms and AMESim.

Three sets of results are provided. First, focus is put on the importance of crossover frequency. Then improvement made by gain scheduling is shown. Finally, we show the interest of controlling the lateral velocity.

5.1 $\mathcal{H}_\infty$ controller only

Here we compare a controller designed at 10Hz and another one designed at 10^{-1}Hz. The longitudinal speed is shown in Fig. 6. The controller designed at a high-frequency

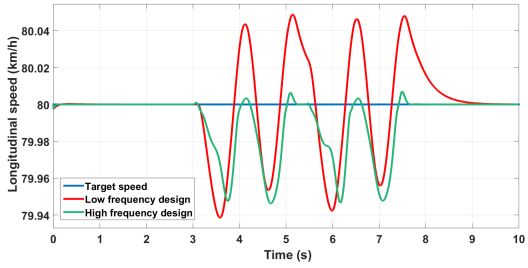

Figure 6: Longitudinal velocity control with different crossover frequencies.

is better as expected. A loss of precision and stability is noticed for the low-frequency designed controller especially in the yaw rate control (Fig. 7).

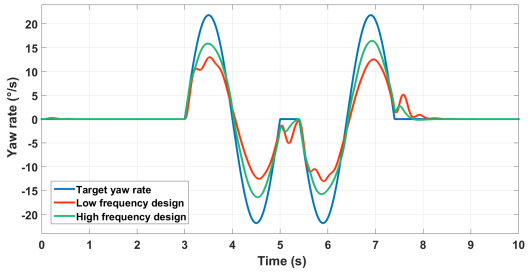

Figure 7: Yaw rate control with different crossover frequencies.

To test the robustness of the high-level control, we change the vehicle parameters regarding the mass and inertia by 20%, and wheelbase by 7%, and also tire parameters regarding the cornering stiffness by 40% in AMESim®, while we keep the same parameters of the high-frequency designed controller in Simulink®. We obtain the Fig. 8. We can see

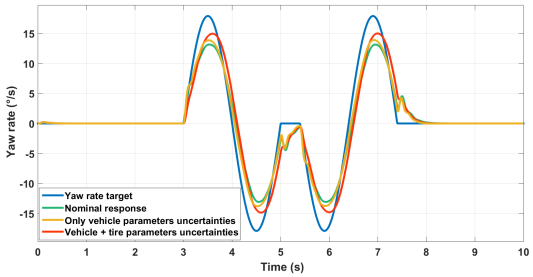

Figure 8: Different controllers for the yaw rate.

that as long as only vehicle parameters are concerned, the vehicle exhibits almost the same performance regarding yaw rate tracking. When we change considerably the tire cornering stiffness, the uncertainties effects become noticeable. The vehicle behavior remains although acceptable. This was expected as the high-level controller determines the motion of the vehicle's center of gravity. Tire influence is managed rather by the control allocation and the low-level control. Robustness at these downstream layers should be improved.

We redo the maneuver with the same steering wheel input but with the reduced longitudinal speed of 20km/h. Results are plotted in Fig. 9. The controller designed using op-

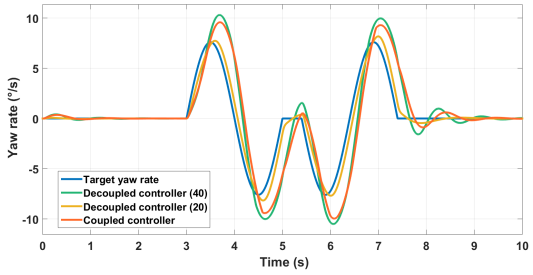

Figure 9: Different controllers for the yaw rate.

erating points at a longitudinal speed of 20km/h exhibits better performance than a controller designed using operating points at a longitudinal speed of 40 km/h for example. This shows that the controller performances are closely related to the operating points used for linearization. Moreover, for these slow dynamics, a coupled controller has the best performance. This confirms the pre-study carried out in Section 3. Bode diagrams were used to choose the structure of off-diagonal controllers. We can conclude that no fixed operating points can be used for all cases, and no fixed architecture using the $\mathcal{H}_\infty$ only is satisfying.

5.2 Gain-scheduled $\mathcal{H}_\infty$ controller

Here state-feedback used for closed-loop control and also as scheduling variable for controller parameters. The previous maneuver is repeated for various longitudinal speed values. Satisfying performance for the yaw rate control are

ensured in different cases where in Fig. 10 we show only the performance for two different speed values for more clarity.

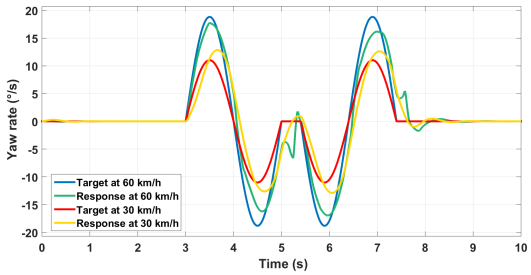

Figure 10: Various speed control using GS $\mathcal{H}_\infty$.

However, we can remark the odd behavior of the vehicle at the most difficult dynamics changes, especially we change rapidly the direction. The behavior also changes from a speed value to another. This may be due to the fact that we only used lookup tables with a basic interpolation algorithm for the different parameters of the controller in the gain-scheduling framework. Another way to tackle the problem is to rather parameterize the controller gains as a polynomial function, and then tune the polynomial coefficients at the different operating points. The order of the polynomial can be increased to add more flexibility. The controller gains may be less accurate at the operating points compared to the lookup tables, but the switch from a behavior to another is softer. This would be investigated in an upcoming research.

5.3 Relevance of lateral velocity control

The lateral velocity control results were kept to the end to discuss their relevance. The Gain-Scheduled controller is used here. Two behaviors are compared. We first use the nominal bicycle model for a conventional behavior, and then minimize the yaw rate while keeping the same target for the lateral speed. The goal is to have a lateral transitional behavior that could be beneficial for obstacle avoidance and stability. The lateral velocity control is illustrated in Fig. 11 and the yaw rate in Fig. 12. The controller is able to

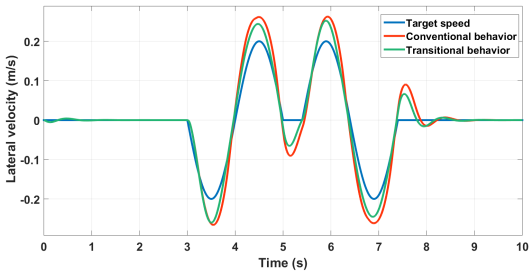

Figure 11: Lateral speed control using GS $\mathcal{H}_\infty$.

generate both behaviors by changing the reference. It should be noted that for a vehicle equipped by rear steering control, stability envelopes should be redefined. In fact, in the literature, stability is more related the vehicle sideslip angle and its time derivative which is called the $\beta - \dot{\beta}$ plane [20]. Here, $\beta = \frac{V_y}{V_x}$ is the vehicle's sideslip angle. A high value of this ratio in conventional vehicles means a loss of control of the vehicle. However, for a 4-wheel steering vehicle, this can represent only a lateral transitional behavior.

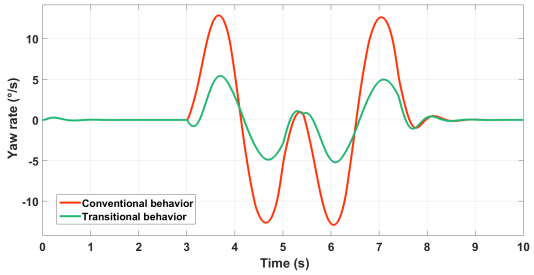

Figure 12: Yaw rate control using GS $\mathcal{H}_\infty$.

6. OPEN CHALLENGES

A methodology of designing robust controllers has been presented. Controllers exhibit satisfying performances with respect to vehicle parameters uncertainties. External changes as wind are usually considered a disturbance that can be rejected by means of the closed-loop. However, certain parameters can influence rapidly the vehicle behavior and even robust controllers may not be sufficient.

6.1 Friction Estimation

One of the major challenges of ground vehicle control is friction estimation. Potential of tires depends on the road/tire interface. This interface is quantified by the coefficient of friction μ [14]. As it was shown in [21], tire behavior is highly nonlinear and changes with different roads. Not only the control should be reconfigurable but also the reference model should be updated. In [22], a sliding mode observer have been designed depending on Dugoff tire model [23]. This latter shows good precision in the linear zone of tire force. It does not provide accurate information about the tire/road interface maximum potential. The maximum potential is actually the most needed estimation in vehicle motion control as authors in [24] have cited. In fact, the global chassis control aims to benefit from the overall potential of the vehicle, but without jeopardizing the vehicle stability by exceeding the limits of friction. Recently, data-based techniques have received more attention. For example, an Auxiliary Particle Filter (APF) have been combined with the Iterated Extended Kalman Filter (IEKF) in [25]. Experimental tests showed promising results.

6.2 Motion Feelings

Another challenge regarding vehicle motion control is the influence on the generated feelings. This is extremely important especially for autonomous vehicles, as it would contribute on their acceptance by the society if a confidence feeling is ensured [26]. In this context, over-actuated vehicles present an interesting opportunity to accelerate autonomous vehicles development. In fact, control allocation algorithms offer the possibility to solve online multi-objective problems [18]. One of the objectives could be then motion feelings by formulating an acceleration-dependent objective to fulfill [27]. The major problem is that motion has different effects on people with different profiles. The command should be personalized to fit best passengers preferences. This is one of the main reasons of the introduction of the lateral transitional behavior in this paper. It should be noted also that this behavior can be accepted for autonomous vehicles, but can be rather unexpected and therefore scary while driving.

Different strategies may be required when switching from a driving mode to another.

7. CONCLUSIONS

We focused in this paper on the high-level controller that should be adopted in vehicle motion control. In contrast with most researches that favour either complex robust controllers based on simplified vehicle models or simplified controllers based on a decoupled complex vehicle, here a structural $\mathcal{H}_\infty$ synthesis has been carried out in a MIMO framework based on a four-wheeled vehicle model. Control allocation techniques have been chosen to ensure optimal coordination between chassis systems.

Co-simulation results show better control performances for coupled motion variables. Not only the yaw rate is controlled while minimizing the influence on the longitudinal speed, but also the lateral velocity is separately controlled, providing additional motion behaviors. For good measure, robustness in a wider operation range is ensured thanks to the Gain-Scheduled $\mathcal{H}_\infty$ control. However, the use of better adaptive real-time friction estimator may enhance the vehicle's safety in case of unexpected events.

Future works consist on embedding this control logic into a real vehicle. We expect from experimental results a better understanding of the impact of the high-level control on the vehicle's behavior and its influence on passengers' feelings.

8. REFERENCES

[1] A. Soltani. *Low Cost Integration of Electric Power-Assisted Steering with Enhanced Stability Program*. PhD thesis, Cranfield University, 2014.

[2] P. Reinold and A. Traechtler. Closed-loop control with optimal tire-force distribution for the horizontal dynamics of an electric vehicle with single-wheel chassis actuators. In *2013 American Control Conference*, pages 2159–2164, June 2013.

[3] A. Chebly, R. Talj, and A. Charara. Coupled longitudinal and lateral control for an autonomous vehicle dynamics modeled using a robotics formalism. *IFAC-PapersOnLine*, 50(1):12526–12532, 2017. 20th IFAC World Congress.

[4] S. Skogestad and I. Postlethwaite. *Multivariable Feedback Control: Analysis and Design, 2nd Edition*. John Wiley & Sons, 2001.

[5] S. Yim. Coordinated control with electronic stability control and active steering devices. *J. of Mechanical Science and Technology*, 29(12):5409–5416, 2015.

[6] Y. He et al. C. Feng, N. Ding. Control allocation algorithm for over-actuated electric vehicles. *J. Cent. South Univ.*, 21:3705–3712, 2014.

[7] L. Dugard J.J. Martinez-Molina P. Gaspar M. Doumiati, O. Sename and Z. Szabo. Integrated vehicle dynamics control via coordination of active front steering and rear braking. *European Journal of Control*, 19(2):121–143, 2013.

[8] Y. Li S. Zhao and X. Qu. Vehicle chassis integrated control based on multimodel and multilevel hierarchical control. *Mathematical Problems in Engineering*, 2014, 2014.

[9] E. Bristol. On a new measure of interaction for multivariable process control. *IEEE Transactions on Automatic Control*, 11(1):133–134, January 1966.

[10] D. Wang B. Shyrokau and M. Lienkamp. Integrated vehicle dynamics control based on control allocation with subsystem coordination. 2013.

[11] G. Scorletti and V. Fromion. *Automatique fréquentielle avancée*. École Centrale de Lyon, 2009.

[12] M. Kissai, B. Monsuez, A. Tapus, and D. Martinez. A new linear tire model with varying parameters. In *2017 2nd IEEE International Conference on Intelligent Transportation Engineering (ICITE)*, pages 108–115, Sept 2017.

[13] M. Kissai, B. Monsuez, and A. Tapus. Review of integrated vehicle dynamics control architectures. In *2017 European Conference on Mobile Robots (ECMR)*, pages 1–8, Sept 2017.

[14] H.B. Pacejka. *Tyre and Vehicle Dynamics, Second Edition*. Elsevier, Butterworth-Heinemann, 2006.

[15] P. Apkarian and D. Noll. Nonsmooth h∞ synthesis. *IEEE Transactions on Automatic Control*, 51(1):71–86, Jan 2006.

[16] W. J. Rugh and J. S. Shamma. Research on gain scheduling. *Automatica*, 36(10):1401–1425, 2000.

[17] Tor A. Johansen and Thor I. Fossen. Control allocation - a survey. *Automatica*, 49:1087–1103, 2013.

[18] O. Harkegard. Efficient active set algorithms for solving constrained least squares problems in aircraft control allocation. In *Proceedings of the 41st IEEE Conference on Decision and Control*, volume 2, pages 1295–1300, Dec 2002.

[19] M. Bodson. Evaluation of optimization methods for control allocation. *Journal of Guidance, Control, and Dynamics*, 25(4):703–711, 2002.

[20] M. A. Selby. *Intelligent Vehicle Motion Control*. PhD thesis, University of Leeds, 2003.

[21] M. Burckhardt. *Fahrwerktechnik: Radschlupf-Regelsysteme*. Vogel-Verlag, 1993.

[22] N. Patra and K. Datta. Observer based road-tire friction estimation for slip control of braking system. *Procedia Engineering*, 38:1566–1574, 2012. International Conference on Modelling Optimization and Computing.

[23] P. Fancher H. Dugoff and L. Segel. *Tire Performance Characteristics Affecting Vehicle Response to Steering and Braking Control Inputs*. Highway Safety Research Institute of Science and Technology, The University of Michigan, Michigan, technical report, CST 460, 1969.

[24] M. Fliess J. Villagra, B. d'Andréa-Novel and H. Mounier. A diagnosis-based approach for tire-road forces and maximum friction estimation. *Control Engineering Practice*, 19(2):174–184, 2011.

[25] Y.-H. Liu, T. Li, Y.-Y. Yang, X.-W. Ji, and J. Wu. Estimation of tire-road friction coefficient based on combined apf-iekf and iteration algorithm. *Mechanical Systems and Signal Processing*, 88:25–35, 2017.

[26] D.P. Stormont. Analyzing human trust of autonomous systems in hazardous environments. In *Proc. of Twenty-Third AAAI Conference on Artificial Intelligence*, pages 27–32, 2008.

[27] F. M. Raimondi and M. Melluso. Fuzzy motion control strategy for cooperation of multiple automated vehicles with passengers comfort. *Automatica*, 44(11):2804–2816, 2008.